Automatic Detection and Characterization of Rockfalls at the Barry Arm Landslide, Prince William Sound, Alaska

by
Henry Chandler

A thesis accepted and approved in partial fulfillment of the
requirements for the degree of
Master of Science
in Earth Sciences

Thesis Committee:
Josh Roering, Chair
Lief Karlstrom, Member
Valerie Sahakian, Member

University of Oregon
Spring 2026

© Copyright, 2026, Henry Chandler

THESIS ABSTRACT

Henry Chandler
Master of Science in Earth Science
Title: Automatic Detection and Characterization of Rockfalls at the Barry Arm Landslide, Prince William Sound, Alaska

Rockfalls are common hazards in steep terrain, driven by diverse environmental forcings. Despite their significance, automated detection and attribution of rockfalls remains challenging. Here, we present a >3-year catalog of rockfall events at the Barry Arm landslide in Prince William Sound, Alaska, an active slow-moving slide with tsunamigenic potential. Using an infrasound array paired with broadband seismometers and a meteorological station, we automatically classified and manually verified 424 rockfall events from September 2022 to December 2025. Factors that influence temporal variations in rockfall activity include deep-seated landslide motion, frost weathering cycles, and precipitation. By combining geomorphic mapping and physics-based rockfall runout modeling, we successfully reproduced event duration and back azimuth trends observed in the infrasound rockfall catalog. These results demonstrate the ability of infrasound to classify and detect rockfalls through time, and represent a novel approach for coupling geophysical monitoring, topographic analysis, and rockfall modelling in remote, hazard-prone environments.

ACKNOWLEDGEMENTS

I deeply thank Professor Josh Roering for all his advising and technical help throughout my degree and project. In addition, special thanks to Dr. Liam Toney and Dr. John Lyons for providing invaluable information and guidance throughout my process of learning infrasound and familiarizing myself with the Barry Arm. Finally, I'd like to thank Maryn Sanders for her support with RAMMS::Rockfall.

TABLE OF CONTENTS

Chapter	Page
1. INTRODUCTION	07
2. METHODS	09
2.1 Study Area: Barry Arm Landslide	09
2.2 Geophysical and Climate Sensors	09
2.3 Remote Sensing and Topographic Data	12
2.4 Modelling with RAMMS	12
3. RESULTS	14
3.1 Rockfall Catalog and Temporal Variations	14
3.2 Geomorphic Mapping and RAMMS Simulations	15
4. DISCUSSION	18
4.1 Environmental Forcings	18
4.2 Topographic Influence on Rockfall Trajectory	19
4.3 Infrasound as a Detection Tool	20
5. CONCLUSION	20
DATA AVAILABILITY	21
APPENDIX: ADDITIONAL FIGURES AND PROCESSES	22
REFERENCES CITED	26

LIST OF FIGURES

Figure Page

1. Maps of the study region and instruments 09
2. Infrasound signal of an event occurring at 13:37:28 UTC on April 29, 2023..... 10
3. Infrasound and seismic data of 2 high quality detected events..... 11
4. Rockfall catalog featuring high and medium quality events 15
5. Rockfall catalog with environmental conditions..... 16
6. Analysis of detected and modeled rockfall catalogs..... 17

A1. Three examples of infrasound signals that meet the automatic detection criteria..... 22

A2. Catalog of all events identified by the infrasound detection methods before elimination by back azimuth, snow cover, and signal quality..... 22

A3. Two examples of infrasonically detected events of various quality with their associated seismic data..... 23

A4. Comparing trends in back azimuth and event duration..... 23

A5. Analysis of boulder length distribution..... 24

A6. Trajectories of all modeled rockfalls in RAMMS..... 24

Text A1 25

1. INTRODUCTION

In steep rocky terrain, rockfalls are rapid mass movements of discrete rock fragments that sculpt landscapes and constitute a significant hazard (Whalley, 1984). Whereas rockfall initiation and movement are rapid, preconditioning for failure can be a slow process involving rock deformation caused by highly diverse forcings (Krautblatter and Dikau, 2007; McColl, 2012). Previous studies suggest that rockfalls can originate from deglaciation (McColl, 2012), intense rainfall (Krautblatter and Moser, 2009), thermal cycles (Collins and Stock, 2016), ground motion (Keefer, 1984), and frost weathering (Matsuoka, 2008). In cold environments, frost weathering, which involves cryosuction, ice segregation, volumetric expansion, and subsequent thaw is a commonly cited trigger for rockfall activity (Matsuoka, 2001; Krautblatter and Moser, 2009; Imaizumi et al., 2025). Volumetric expansion can result in the formation of new cracks and/or the propagation of existing ones (Murton et al., 2006; Draebing and Krautblatter, 2019). This mechanism is vigorous when rock mass temperatures are between -8°C and -3°C such that mountain-scale rockfall activity and erosion exhibit strong altitudinal patterns (Hales and Roering, 2009; Rempel, 2016; Rengers, 2020). Warming and thaw following prolonged periods of frost weathering has been shown to increase rockfall rates for 5-15 days (Matsuoka and Sakai, 1998). Despite decades of investigation, direct documentation and attribution of rockfall initiation mechanisms remains difficult due to the sporadic and often remote nature of rockfalls. Past rockfall identification techniques include observation of deposits on snow (Matsuoka and Sakai, 1998), witnessing (Gardner, 1983), topographic change detection (Williams et al., 2018), and timelapse camera monitoring (Matsuoka, 2019). More recent work has demonstrated the capability of seismic and acoustic sensors for detecting rockfalls (Zimmer and Sitar, 2015), which are capable of continuous monitoring with high temporal resolution. The ability of these geophysical sensors to constrain spatial patterns of rockfall activity has not been assessed, particularly within the context of rockfall source areas, pathways, and deposits defined by the accumulation of rockfalls on bedrock slopes (Wachino et al., 2026).

Infrasound sensors record atmospheric pressure waves with frequency less than 20 Hz, which is below the audible range (Fee and Matoza, 2013). These low frequency infrasound waves propagate long distances, allowing the sensors to detect sources hundreds of kilometers

away (Allstadt et al., 2018). An array of sensors (3 or more) can identify the speed and incoming direction of pressure waves propagating across the array (Matoza et al., 2007). While infrasound sensors have been used to detect avalanches (Johnson et al., 2021, Watson et al., 2022; Watson et al., 2026), debris flows (Kogelnig et al., 2014; Coviello et al., 2019; Liu et al., 2022), and volcanic eruptions (Fee and Matoza, 2013; Lyons et al., 2024; Watson et al., 2022), few studies have applied these methods to rockfalls (Johnson and Ronan, 2015; Zimmer and Sitar, 2015). The potential for long monitoring campaigns and high spatial and temporal resolution afforded by a local (< 2 km from the source) infrasound array makes this an attractive method to detect rockfalls, diagnose triggering mechanisms, and assess their transport pathways.

In this study, we generate a catalog of rockfall events using an automated classification scheme that draws upon infrasound and seismic data at the Barry Arm landslide in Alaska. We evaluate the capability of the infrasound array to characterize rockfall events and assess how movement of the landslide and environmental forcings regulate rockfall activity. Our results support the utility of infrasound sensors coupled with geomorphic mapping and runout modeling to monitor and characterize rockfall initiation and runout pathways.

2. METHODS

2.1 Study area: Barry Arm landslide

To investigate the ability of infrasound sensors to decipher the topographic context and environmental forcings of rockfall events, we used a >3-yr long dataset that includes an infrasound array, two seismometers, and a hydrometeorological site located near the terminus of the Barry Glacier in Prince William Sound, Alaska, USA (Figure 1). In the Barry Arm fjord, recent deglaciation and debuttressing has exposed a large (580 Mm^3) deep-seated, slow moving landslide on the western valley wall (Schaefer, 2023). Identified in 2019, the landslide is extensively monitored owing to its tsunamigenic potential upon catastrophic failure (Dai et al., 2020; Barnhart et al., 2021). The landslide experienced periods of rapid and extensive motion from August to November 2022 of 20-80 mm day^{-1} and from September to October 2023 of 10-20 mm day^{-1} but has remained relatively inactive more recently (Dow et al., 2025).

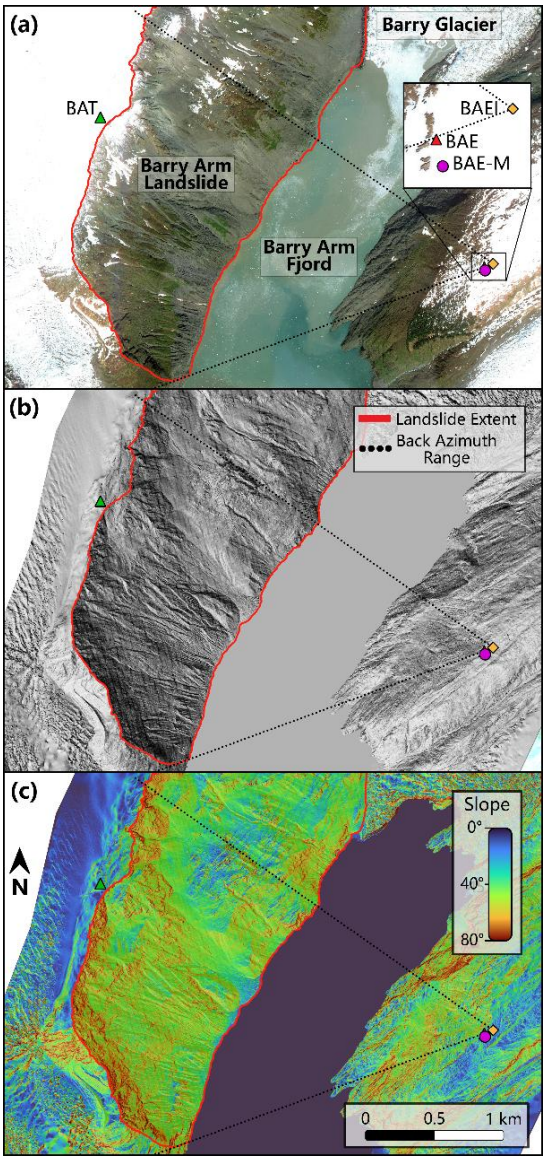


Figure 1. Maps of the study region and instruments. (a) Google Earth imagery from 2017-05-29. (b) 2020 DGGS lidar DEM (1m resolution). (c) Lidar DEM overlaid with mapped topographic classifications. (d) Slope map derived from the lidar imagery.

2.2 Geophysical and climate sensors

In September 2022, the United States Geological Survey (USGS), the Alaska Division of Geological & Geophysical Surveys (DGGS), and the Alaska Earthquake Center (AEC), coordinated installation of an infrasound array (BAEI), broadband seismometers (BAT and BAE), and a meteorological station (BAE-M). All sensors were positioned across the fjord ~2km away from the

landslide except BAT, which was located above the landslide headscarp (Figure 1). BAEI consists of 6 infrasound sensors in an array configuration with ~50 m spacing.

For infrasound processing, we apply a bandpass filter of 0-30 Hz to the raw data and use ordinary least squares beamforming to measure the similarity of the signal recorded by each individual sensor (coherence), the speed of the pressure wave passing over the array (trace velocity), and the incoming direction of the pressure wave (back azimuth) at each window (Bishop et al., 2020, Figure 2). We use an 8 second window with 50% overlap. To identify

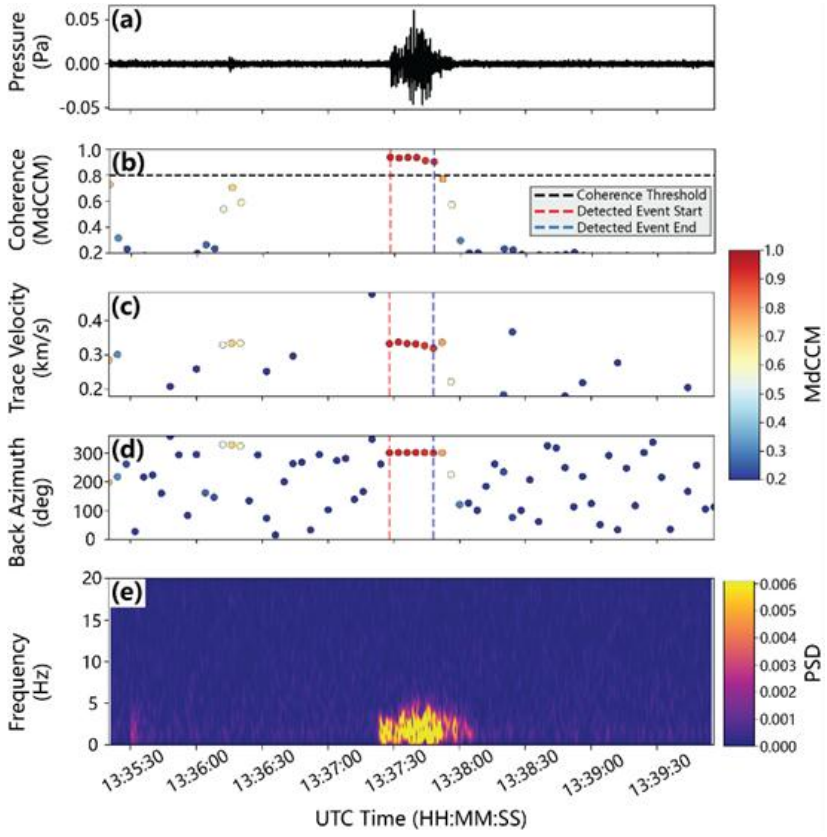


Figure 2. Infrasound signal of an event occurring at 13:37:28 UTC on April 29, 2023. (a) Infrasound waveform from array element 01. (b) Median cross-correlation maximum (MdCCM) coherence metric. Coherence is a measure of similarity between waveforms recorded at each array element. (c) The apparent speed (trace velocity) of the sound wave propagating across the array. (d) The incoming direction of the signal as it propagates across the array. (e) Spectrogram of the infrasound signal from element 01. Units for the power spectral density (PSD) are Pa^2/Hz (Figure A1).

possible rockfall events with BAEI data, we set the following: 1) a coherence threshold of 0.8 for 16 seconds (3 consecutive window measurements), 2) trace velocity from 300-400 m/s, and 3) back azimuth values that identify events emanating from the main slide body, which is 250° to 305° back azimuth from BAEI (Figure A2). For each event that emerges from these criteria, we record the initial back azimuth value and the duration of the event and compute a spectrogram. Considering that characterizing events with back azimuth gives no distance from BAEI, it is possible that signals originating beyond the landslide headscarp can make it through our automatic detection criteria.

For each event resulting from our infrasound detection criteria, we use seismic data (with a 0-20 Hz bandpass filter applied) recorded at BAT and BAE for verification and quality assessment. We visually inspected the infrasound and seismic waveforms and associated spectrograms for each event (Figure 3). High quality events have strong infrasound and seismic signals with coincident timing that fall within the expected frequency range of rockfalls (Allstadt et al., 2018). Proper signal arrival times are set by site geometry and medium of travel and here that results in a systematic time delay between the seismic signal and infrasound signal of about 6 seconds. Medium quality events meet all of the same requirements of the high quality events

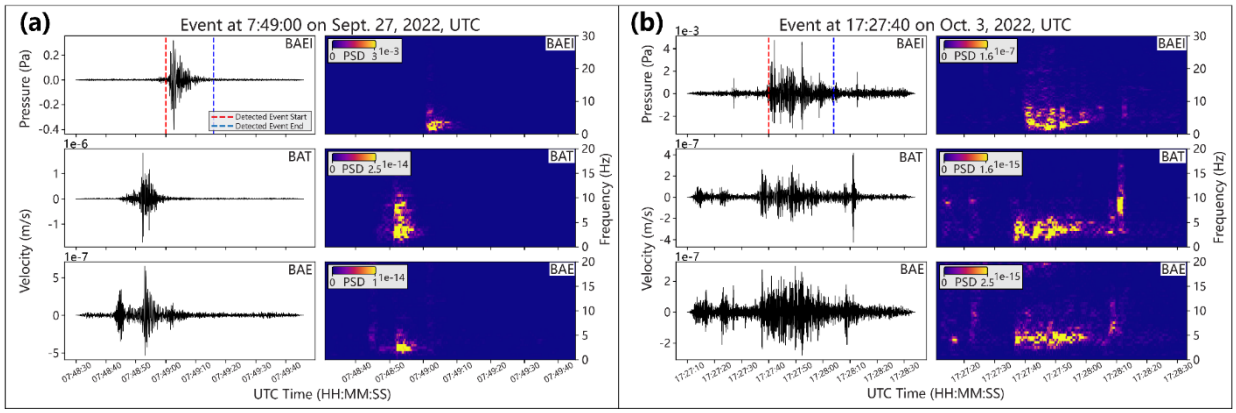


Figure 3. Infrasound and seismic data of 2 high quality detected events. (a) Event occurring on Sept. 27, 2022. (b) Event occurring on Oct. 3, 2022. Both events show proper frequency signatures and event timing. Units for the BAEI PSD are Pa^2/Hz. Units for the seismometer PSD are $(m/s)^2/Hz$. This waveform and spectrogram data is what we used to evaluate signal quality. Figure A3.

but have signals that are slightly mistimed or that are partially obscured by noise. Poor quality events lack a combination of coincident timing, appropriate frequency, or are too noisy to decipher. Our rockfall catalog only includes high and medium quality events, although considering only high quality events would not significantly change our results (Figure A4). While signals emanating from beyond the landslide headscarp will likely meet the criteria of our automatic detection scheme, it is very unlikely they will display the coincident timing required to be deemed high or medium quality events.

From BAE-M, we gathered daily average, minimum, and maximum temperature and daily rainfall. We used the temperature data to calculate a weekly tally of days within the frost weathering window defined by -8 to -3°C for comparison with our rockfall event catalog. This temperature range from -8 to -3°C will serve as a proxy for frost damage (Sanders et al., 2012).

2.3. Remote sensing and topographic data

To analyze how site topography and surface features may affect rockfall pathways, we used a high-resolution (5 cm) structure from motion (SfM) orthoimage and a 1m resolution lidar digital elevation model (DEM) from 2020 (Daanen et al., 2021). Using the lidar DEM, we calculated slope and roughness to identify zones of likely rockfall initiation and inform our geomorphic mapping (Glenn et al., 2006). We also used the high-resolution orthoimage to document the location, size, and shape of 100 boulders that accumulated along the lower portions of the slide and reflect the endpoints of rockfall activity.

Because of avalanche abundance during winter and snow cover suppressing rockfall activity, we visually inspected near-daily Planet Labs imagery to determine time intervals when the landslide was fully covered in snow. Our inventory is limited to time periods when the entire landslide surface is free of snow.

2.4 Modelling with RAMMS

To test the ability of our infrasound rockfall catalog to distinguish rockfall location and duration, we compared back azimuth values and duration trends with modeled rockfalls using

RAMMS::Rockfall (Christen et al., 2012; Leine et al., 2014). RAMMS is a physics based rockfall modelling software that allows the user to specify topography, ground type, rockfall source location, rockfall size and shape, and source orientation. To implement RAMMS, we used the 2020 DGGS 1m resolution lidar DEM to represent the morphology of the Barry Arm landslide. We identified rockfall source areas as terrain with slopes values exceeding 60 degrees (Dibiase et al., 2012; Wachino et al., 2026). Using the manually mapped boulders, we created a boulder length (long axis) distribution and identified the 25th, 50th, 75th, and 90th percentiles and then selected mapped boulders that most closely matched these lengths (Figure A5). We then used measurements to model the size, shape, and mass of these representative boulders for input into RAMMS. We used Planet Labs imagery to identify ground cover classification, which consisted of coarse talus and vegetated talus. Finally, we specified 1,000 source locations randomly distributed within the >60° rockfall source areas and selected 5 random starting orientations for each of the 4 representative boulders. The resulting simulation generated 20,000 individual rockfalls with locations and complete trajectories denoted (Figure A6, Text A1).

3. RESULTS

3.1 Rockfall catalog and temporal variations

Our analysis of BAEI infrasound data spanning September 6, 2022 to December 31, 2025 resulted in 582 individual rockfall event detections. Upon manual verification, we eliminated 158 events due to poor quality and focused our analysis on the remaining 424 events with suitable quality. Of those 424 events, 159 (37.5%) had coinciding seismic data available from both BAT and BAE for verification, 61 (14.4%) coincided with available seismic data from either BAT or BAE, and the remaining 204 (48.1%) occurred at times with no seismic data available. The availability of seismic data is primarily driven by battery life constraints. Given the consistent infrasound signatures, we retained these 204 events for analysis.

Aside from omitted periods in the rockfall record owing to periods of comprehensive snow cover that span early November to late March, we observed temporal variations in activity that may reflect movement of the Barry Arm landslide as well as seasonal climate fluctuations (Figure 4). Our results show abundant rockfall activity during the two periods of slide movement from August to November 2022 (20-80 mm day^{-1}), and from September to October 2023 (10-20 mm day^{-1}). Rockfall activity is much more frequent during the 2022 period of movement, having 4 separate weeks containing over 5 events, compared to the same period in 2023 where 5 events are exceeded only once. Additionally, in both cases, rockfalls remain abundant in the following spring, although landslide motion is not recorded at these times. While the spring following the 2023 motion does display elevated rockfall frequency, the spring following the 2022 motion is much more active, often exceeding 15 events in a week. These periods of elevated rockfall frequency are followed by less activity in the latter half of 2024 and 2025 when slide motion was negligible and weekly detection totals seldom exceeded 3.

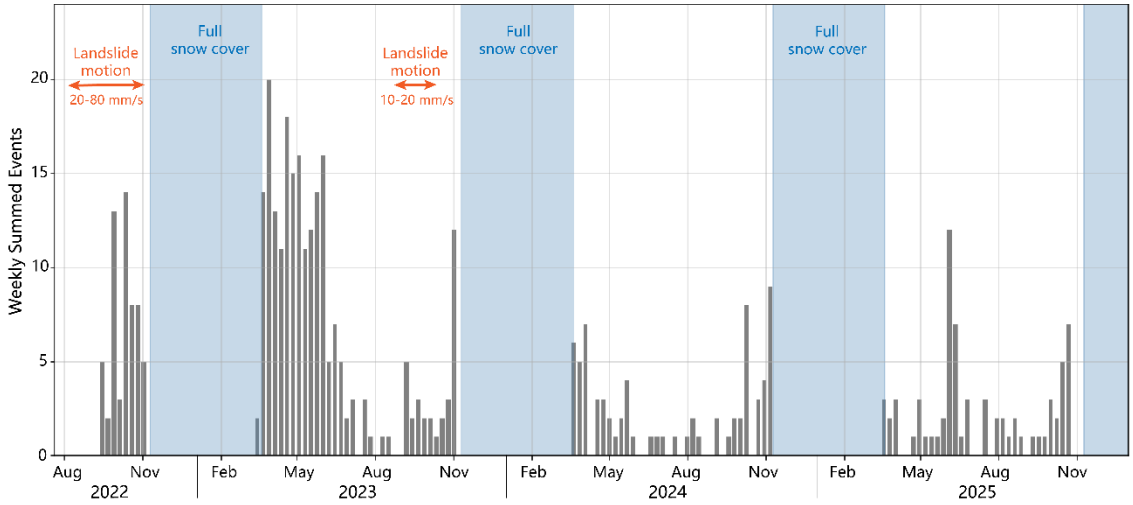


Figure 4. Rockfall catalog featuring high and medium quality events. The Barry Arm landslide saw motion in the fall of 2022 and 2023. Blue shaded regions are periods with full snow cover and although there were events detected during these times, they are not considered in this study.

Our analysis of meteorological station data shows that air temperatures are consistently below zero and often in the frost cracking window (-8 to -3°C) from late fall to early spring, which precedes periods of elevated rockfall activity (Figure 5). Daily rainfall, which tends to peak in late-summer before gradually decreasing in the fall, occasionally coincides with rockfall events in our catalog

3.2 Geomorphic mapping and RAMMS simulations

The Barry Arm landslide zone has heterogeneous topography, consisting of bedrock cliffs, gentle benches, incised channels, and talus slopes (Figure 6). Areas identified as bedrock cliffs exhibit very high slope, high roughness, and sparse channels. Gentle benches and coinciding cliffs exhibited consecutive strips of low and high slope orthogonal to the dip of the

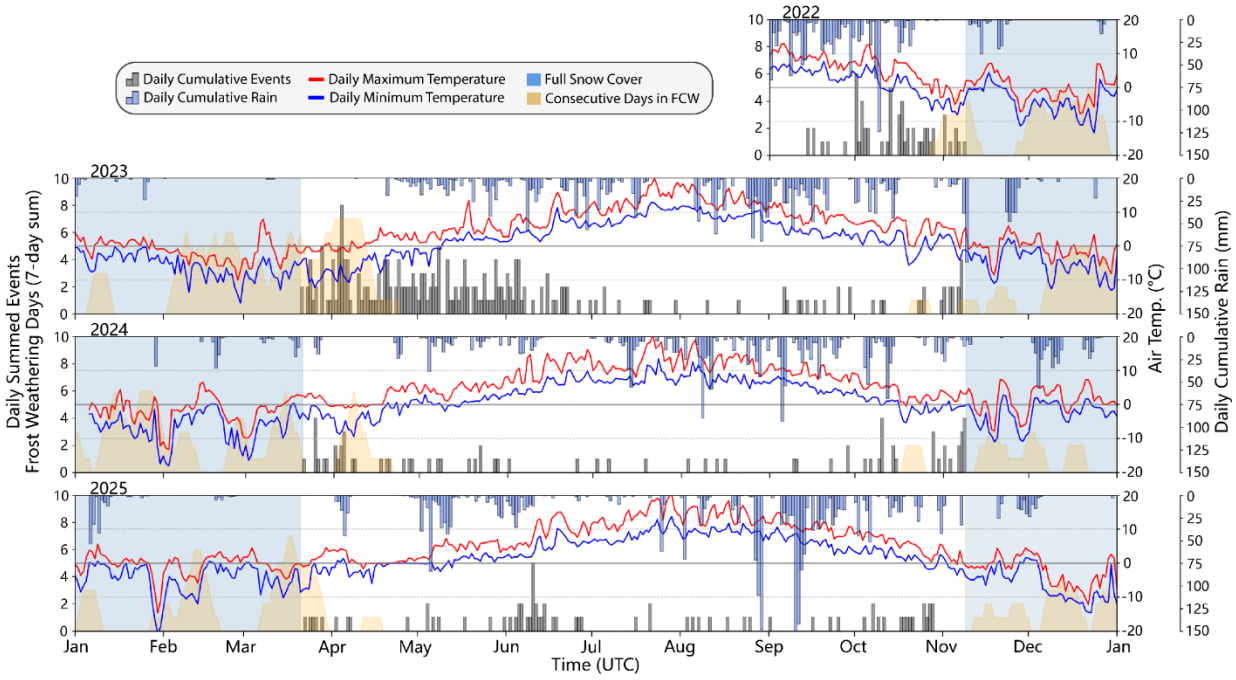


Figure 5. Rockfall catalog with environmental conditions: frost cracking proxy, daily cumulative rainfall, snow cover periods, and daily max and min temperatures. While no rockfalls occurring during full snow cover are analyzed in this study, temperatures show frost cracking damage could be occurring, pre-conditioning the slope for failure upon spring melt.

landslide. Channelized regions often have high slope and visible incised channels. Talus slopes are areas of low roughness and lower slope and exhibit evidence of sediment deposition. We observe steep bedrock cliffs near the headscarp of the landslide which likely serve as rockfall initiation points. At the southern end of the landslide mass, the headscarp declines in elevation, becoming closer to the fjord, making the landslide narrower in the south than it is in the north. Talus deposits appear just below the headscarp in the northern corner of our study area and narrow to a thin chute through the center of the slide before ending as fans at the base of the middle of the slide. Gentle benches appear in 3 primary locations: just below the talus slope on the northern end of the slide, above the talus chute in the center of the slide, and to a lesser degree near the base of the southern part of the slide. The remainder of the slide exhibits channelized characteristics.

The pattern of rockfall initiation back azimuth and event duration display non-uniform trends (Figure 6). We observe that rockfalls initiating at the southern and northern extents of the slide have shorter event durations while the center of the landslide mass features rockfalls of longer duration. The RAMMS modelling shows similar trends to our catalog, specifically, rockfalls initiating in the center of the landslide show long runouts. Likewise, modeled rockfalls with shorter runouts occur on the southern and northern ends of the study area, coincident with locations that exhibit shorter event durations in our catalog.

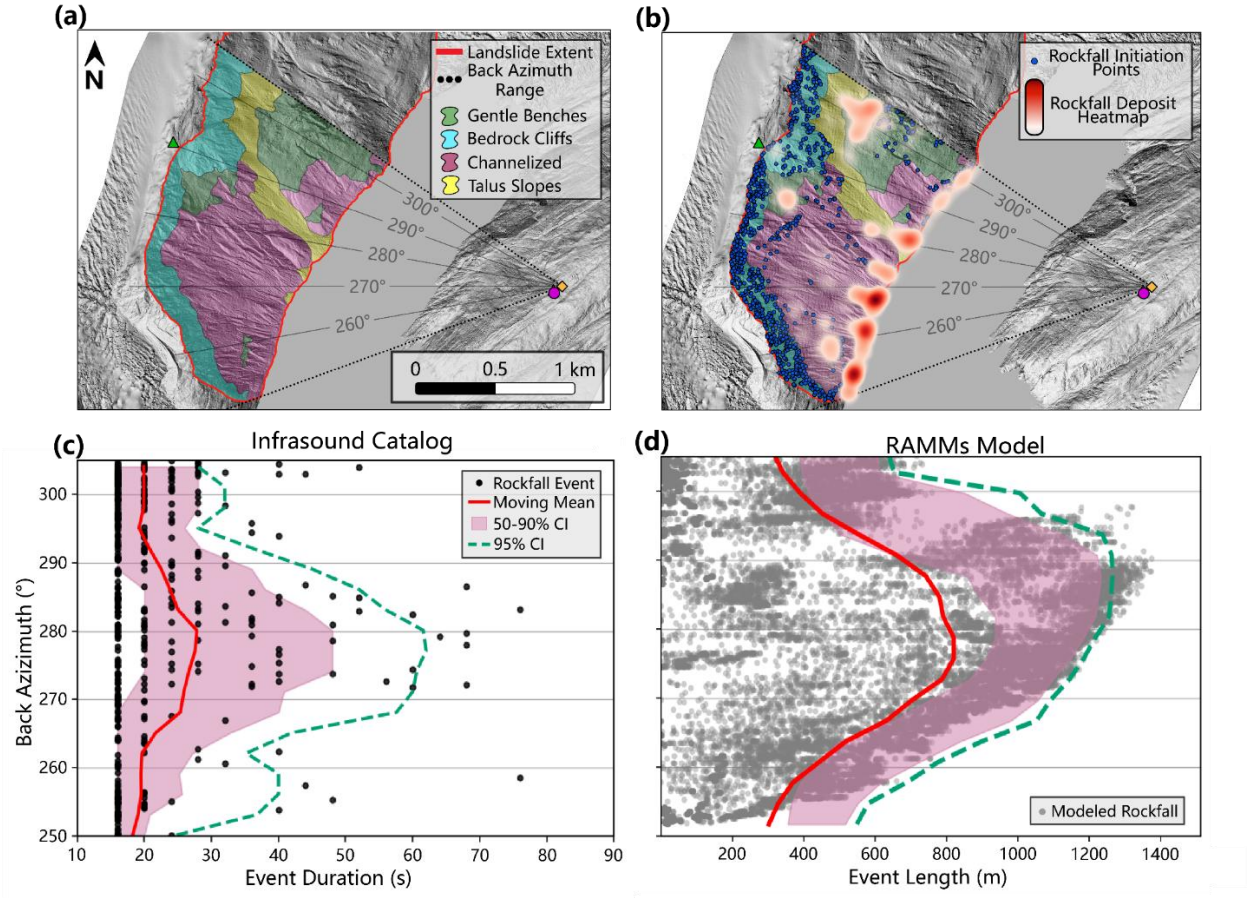


Figure 6. Analysis of detected and modeled rockfall catalogs. (a) Map of the study region with topographic classifications and reference azimuths from BAEI. (b) Spatial distribution of RAMMs modeled rockfall initiation and deposition. (c) Back azimuth and event duration relationship for our rockfall catalog with associated confidence interval (CI) data. (d) Back azimuth and event length relationship for the RAMMs modeled rockfalls.

4. DISCUSSION

4.1 Environmental forcings

We attribute the interannual changes in rockfall frequency to the motion of the Barry Arm landslide, which was active from August to November 2022 and again from September to October 2023. Mass movements tend to become more common following earthquakes owing to damage to bedrock and surface layers, decompaction of soil, and crack dilation and extension (Keefer, 1984; Marc et al., 2015; Fan et al., 2019). These and related rock deformation mechanisms may occur in response to periods of deep-seated movement on the Barry Arm landslide, effectively priming the near-surface to be susceptible to rockfall activity. Landslide motion in 2022 was more extreme, lasting longer and reaching up to 8 times the speed of motion in 2023. This difference in speed could explain the higher frequency of rockfall during and following landslide motion in 2022 compared to 2023.

While we did not analyze any event signals during the winter owing to full snow cover, temperature trends indicate conditions that favor frost cracking. In addition, ice accumulated in near-surface cracks can also bind rock masses together, eventually releasing upon thaw (Matsuoka and Sakai, 1999; Krautblatter et al., 2012; Mamot et al., 2018). This mechanism of frost damage and delayed rockfall following landslide motion is consistent with our observations of increased activity in the spring of 2022 and 2023. Furthermore, the pronounced decline in activity during 2024 and 2025 may reflect the exhaustion of readily destabilized rock mass and deposits generated during the period of rapid movement. As such, movement of the Barry Arm landslide may contribute to elevated rockfall activity for months or longer after becoming dormant. Importantly, our climate analysis uses air temperatures although rock surface temperatures are more relevant for assessing the efficacy of frost weathering because they incorporate the influence of insolation (Collins and Stock, 2016; Draebing and Meyer, 2021).

Additionally, some peaks in rockfall frequency appear to be preceded by peaks in precipitation, most notably in October 2022, November 2023, October 2024, and June 2025. This trend is not consistent, however, as many peaks in rainfall are not associated with subsequent

rockfall activity. A more comprehensive analysis of how environmental forcing and deep-seated movement of the Barry Arm landslide contributes to rockfall activity demands a longer catalog.

4.2 Topographic influence on rockfall trajectory

Using topographic heterogeneity, we modeled the trajectory of rockfalls initiating at different points along the landslide headscarp. Talus fans at the base of the landslide indicate that many rockfalls reach the bottom of the slide mass in these locations. Gentle benches may serve as rockfall traps causing incoming rockfalls to lose energy and deposit on top of existing benches and may also act as rockfall sources on their steeper, downslope margins. Given these observations as well as variations in the amount of steep, cliffy rockfall sources areas, we anticipate rockfalls in the northern and southern ends of the landslide mass to be relatively short, as they are more likely to initiate closer to the bottom of the slide area (southern section) or deposit on gentle benches before reaching the bottom of the slope (northern section). By contrast, rockfalls occurring in the central section have fewer obstacles and are therefore more likely to have long runouts and deposit near the bottom of the slope.

In this study, we employed the novel method of using topographic analysis to predict rockfall runout and confirming with modeled rockfalls to test the ability of the infrasound array to correctly identify rockfall trajectory trends. Our rockfall catalog displays a striking correlation with our topographically based rockfall predictions and RAMMs model. We observe that rockfalls initiating at back azimuths corresponding to talus chutes and debris fans have long event durations and rockfalls with back azimuths coincident with benches exhibit shorter event durations, as seen in the RAMMs model. This result highlights the ability of the infrasound array to both accurately identify rockfall initiation zones and reliably track event duration. While the spatial and temporal resolution are unknown, the positioning of the infrasound (< 2km from the landslide) is such that uncertainty stemming from resolution limitations is negligible. The method can also be used to forecast rockfall initiation and deposition zones and inform the spatial pattern of landscape evolution.

4.3 Infrasound as a detection tool

Our results show the ability of infrasound arrays to identify the timing and orientation of rockfall events, highlighting its potential as a tool to detect and catalog rockfalls and inform mitigation efforts. Although several non-rockfall noise impulses activated our detection algorithm, our manual verification of events with raw data and spectrogram characteristics provides high confidence in our catalog of >400 events. Our use of one infrasound array means that we were unable to uniquely and independently estimate source locations, thus, we cannot eliminate the possibility that our detection scheme includes signals originating beyond the landslide headscarp. However, these signals would lack the expected signal delay between the infrasound and seismometers, and thus likely be eliminated upon manual detection given sufficient data. While the size of our catalog is such that manual verification of events was possible, use of automatic verification processes would be crucial for larger datasets. High quality rockfall events display characteristic frequency signatures and site-specific timing, which trained tools could learn to recognize. Datasets such as our catalog here could serve as training data for machine learning methods, making both the rockfall detection and verification automatic.

5. CONCLUSION

This study used a deep-seated landslide with intermittent activity to test the ability of infrasound sensors to automatically detect and characterize rockfalls over several years. Our catalog of 424 events over >3 years shows that rockfalls occurring on the landslide likely stem from diverse forcings, including: deep-seated movement of the landslide, frost weathering, and precipitation. Our use of geomorphic mapping and rockfall runout simulations for comparison with the location and duration of rockfalls in our infrasound catalog provides a novel methodology for testing and verifying the catalog. The spatial pattern of talus deposits, rockfall chutes, and low-gradient bedrock benches atop the Barry Arm landslide provide key insights on rockfall activity. These results demonstrate that the coupling of geophysical sensors with process-based modeling provides a powerful approach for building monitoring systems and interpreting signals from diverse sources.

DATA AVAILABILITY

Infrasound (BAEI) and seismic (BAT, BAE) waveform data are archived at the IRIS/EarthScope Data Management Center and are publicly available via the IRIS station finder (https://ds.iris.edu/mda/). Meteorological data from the BAE-M station are publicly available through the Alaska Division of Geological & Geophysical Surveys (DGGS) weather station network (https://dggs.alaska.gov/weatherstations/#8). Infrasound array processing was performed using the lts_array package (Bishop et al., 2020; https://github.com/uafgeotools/lts_array). Analysis code, GIS, and RAMMS data produced in this study are archived at https://github.com/henry-chandler/BA_analysis and are freely available.

APPENDIX

ADDITIONAL FIGURES AND PROCESSES

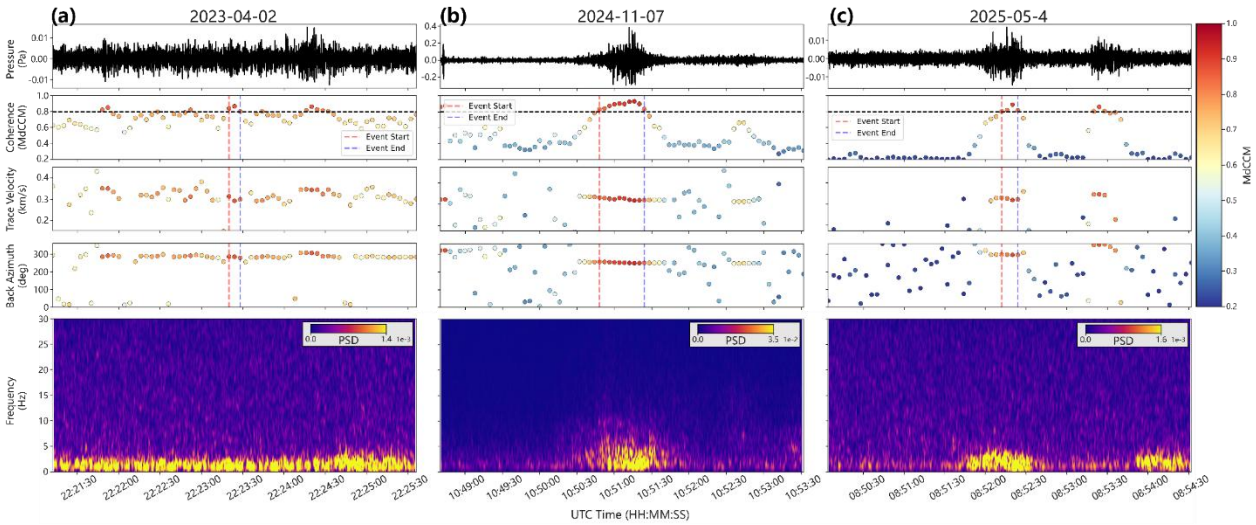


Figure A1. Three examples of infrasound signals that met the automatic detection criteria. The detection in panel (a) does not seem to be associated with a real rockfall, rather a period of high noise. Panels (b) and (c) are likely real events, and thus would pass the manual verification if the available seismic data supports this decision.

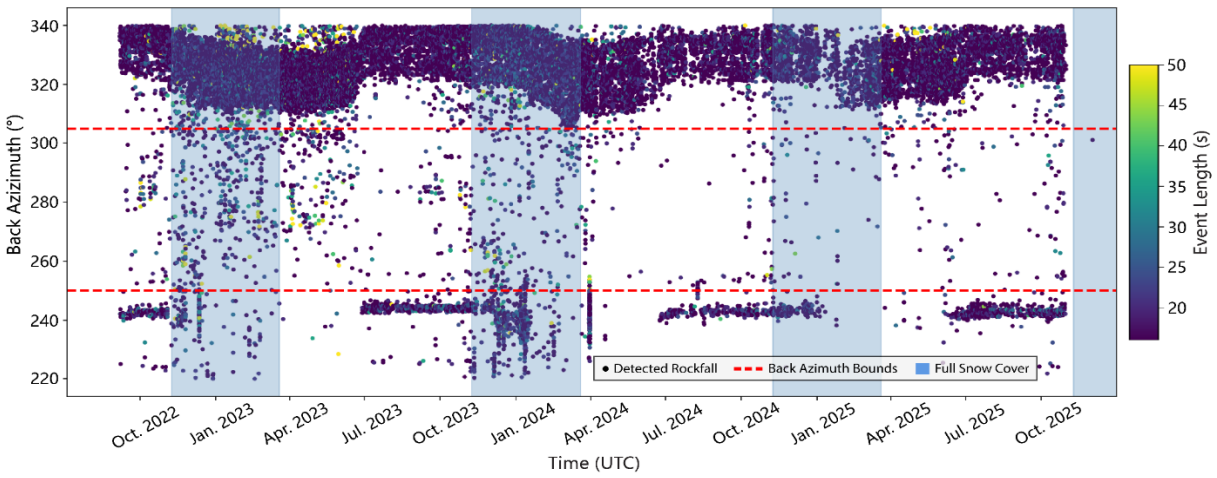


Figure A2. Catalog of all events identified by the infrasound detection methods before elimination by back azimuth, snow cover, and signal quality. The bands of extremely frequent events at the top and bottom of the figure are likely glacier calvings. The thick, oscillating band from back azimuth 310° to 340° is likely from Barry glacier, with the oscillations due to seasonal changes in glacial extent. The thinner, more sporadic band at around 242° is likely glacial calving events from the smaller Cascade glacier. We used the glacial extents observed in this plot to identify the acceptable back azimuth range for rockfall events, eliminating all signals likely originating from glaciers.

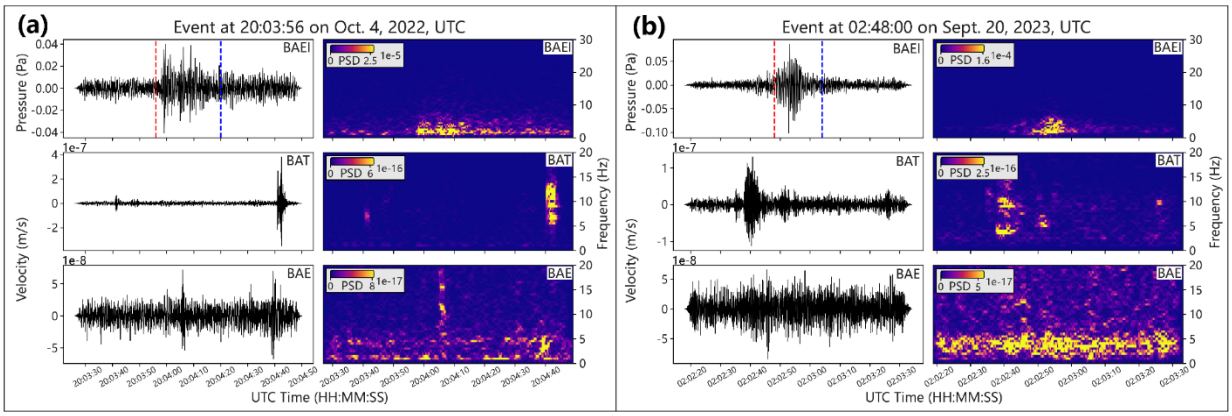


Figure A3. Two examples of infrasonically detected events of various quality with their associated seismic data. (a) shows an event deemed to have poor quality upon manual review. While the infrasound has a clear signal, BAT does not have a corresponding event. (b) shows an event of medium quality. All three sensors show a signal with proper site-specific timing. However, the signal from BAE is covered by strong noise.

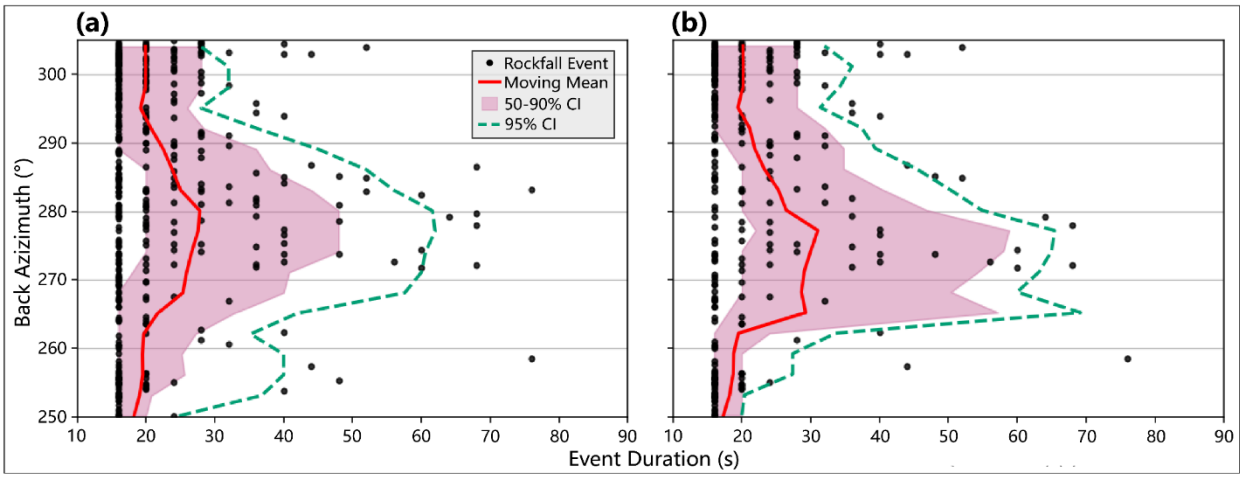


Figure A4. Comparing trends in back azimuth and event duration for our catalog including (a) rockfall events of medium and high quality, and (b) only high quality events. This comparison shows that our catalog of infrasonically detected events displays the same back azimuth and duration trends whether considering events of medium and high quality or only high quality. However, when only considering high quality events, the trend is much more skewed by outliers. Thus, we chose to include events of medium quality to add robustness to the observed trends. It should be noted, however, that the consideration and analysis of solely high quality events would not change the conclusions made in this study.

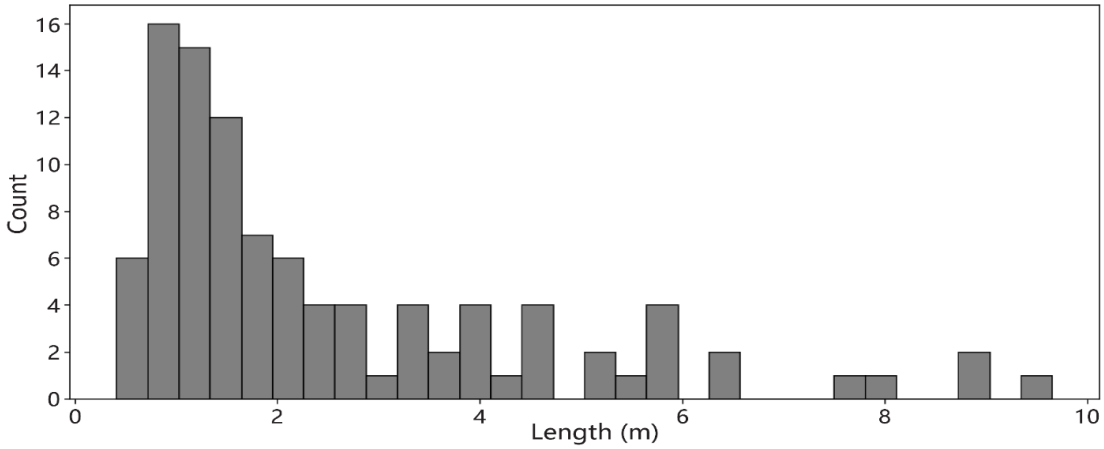


Figure A5. Analysis of boulder length distribution. This plot represents the primary axis length distribution of all 100 manually mapped boulders. Analysis of the distribution shows the 25th, 50th, 75th, and 90th percentiles are 1.08, 1.75, 3.53, and 5.89 m respectively. The real boulders chosen for representation in RAMMS that most closely fit the percentiles had lengths of 1.07, 1.85, 3.21, and 5.91 m. As depth of the boulders was too unreliable to measure due to lidar resolution limitations, we assumed the depth of each boulder to be equal to its width.

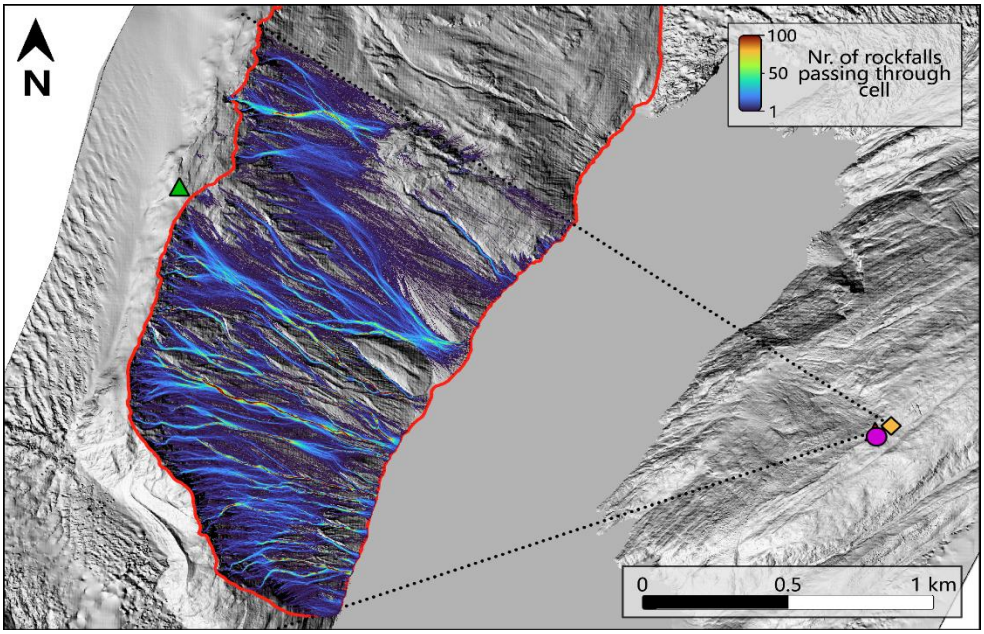


Figure A6. Trajectories of all modeled rockfalls in RAMMS. Many rockfalls deposit halfway down the slope in the northern section, and near the base of the southern section. Both locations feature gentle benches. Rockfalls concentrated in a few, long channels, most notably down the center of the landslide and ending at mapped talus deposits at the base of the slide. This map shows the tendency for rockfalls to deposit when encountering topographic benches, and to run out longer distances when travelling through channelized or talus dominated regions.

Text A1. RAMMS::Rockfall workflow

The 2020 DGGS 1m resolution lidar DEM served as the terrain for our RAMMS simulation. RAMMS allows the categorization of ground type. Using Planetlabs imagery, we classified the slope coarse talus and vegetated talus, and we specified water at the base of the slope. To identify rockfall source areas, we automatically created polygons everywhere the slope exceeded 60°. We specified that rockfalls will initiate from 1,000 unique and discrete points randomly distributed throughout the initiation zone polygons. To inform the modeling of simulated boulders, we mapped 100 boulders on the landslide surface and created a distribution of their primary axes. From the distribution of boulder lengths, we extracted the 25^{th}, 50^{th}, 75^{th}, and 90^{th} percentile lengths, the found mapped boulder that most closely fit those lengths. Using the selected mapped boulder, we found default rock models in RAMMS that most closely fit the boulder shape. We assumed that the depth of each boulder was equal to its width, then used the mapped length, mapped width, and assumed depth to find the volume of each boulder. We then chose a representative density of 2250 kg/m^3 for the boulders (Dai et al., 2020). Finally, we specified that the boulder should be initiated in 5 random rotational orientations. The combination of 1,000 source points, 4 simulated boulders, and 5 random initiation orientations resulted in 20,000 modeled rockfall trajectories.

REFERENCES CITED

Allstadt, Kate E., Robin S. Matoza, Andrew B. Lockhart, et al. "Seismic and Acoustic Signatures of Surficial Mass Movements at Volcanoes." *Journal of Volcanology and Geothermal Research* 364 (September 2018): 76–106. https://doi.org/10.1016/j.jvolgeores.2018.09.007.

Barnhart, Katherine, Ryan Jones, David George, Jeffrey A. Coe, and Dennis M. Staley. *Preliminary Assessment of the Wave Generating Potential from Landslides at Barry Arm, Prince William Sound, Alaska*. Open-File Report. Open-File Report. 2021.

Bishop, Jordan W., David Fee, and Curt A. L. Szuberla. "Improved Infrasound Array Processing with Robust Estimators." *Geophysical Journal International* 221, no. 3 (2020): 2058–74. https://doi.org/10.1093/gji/ggaa110.

Christen, M., Y. Bühler, P. Bartelt, et al. "Integral Hazard Management Using a Unified Software Environment: Numerical Simulation Tool 'RAMMS' for Gravitational Natural Hazards." 2012, 77–86. https://www.dora.lib4ri.ch/wsl/islandora/object/wsl:17955.

Collins, Brian D., and Greg M. Stock. "Rockfall Triggering by Cyclic Thermal Stressing of Exfoliation Fractures." *Nature Geoscience* 9, no. 5 (2016): 395–400. https://doi.org/10.1038/ngeo2686.

Coviello, V., M. Arattano, F. Comiti, P. Macconi, and L. Marchi. "Seismic Characterization of Debris Flows: Insights into Energy Radiation and Implications for Warning." *Journal of Geophysical Research: Earth Surface* 124, no. 6 (2019): 6. https://doi.org/10.1029/2018JF004683.

Daanen, R. P., G. J. Wolken, Katreen Wikstrom Jones, and A. M. Herbst. *Lidar-Derived Elevation Data for Upper Barry Arm, Southcentral Alaska, June 26, 2020*. RDF 2021-1. Alaska Division of Geological & Geophysical Surveys, 2021. https://doi.org/10.14509/30589.

Dai, Chunli, Bretwood Higman, Patrick J. Lynett, et al. "Detection and Assessment of a Large and Potentially Tsunamigenic Periglacial Landslide in Barry Arm, Alaska." *Geophysical Research Letters* 47, no. 22 (2020): e2020GL089800. https://doi.org/10.1029/2020GL089800.

DiBiase, Roman A., Arjun M. Heimsath, and Kelin X. Whipple. "Hillslope Response to Tectonic Forcing in Threshold Landscapes." *Earth Surface Processes and Landforms* 37, no. 8 (2012): 855–65. https://doi.org/10.1002/esp.3205.

Dow, Helen, Brian Collins, Gabriel Wolken, Charles Miles, and Johannes Gassner. "Meteorological Drivers of Seasonal Motion at the Barry Arm Landslide, Prince William Sound, Alaska." Paper presented at European Geosciences Union General Assembly 2025 (EGU25). April 2025. https://doi.org/10.5194/egusphere-egu25-14690.

Draebing, Daniel, and Michael Krautblatter. "The Efficacy of Frost Weathering Processes in Alpine Rockwalls." *Geophysical Research Letters* 46, no. 12 (2019): 6516–24. https://doi.org/10.1029/2019GL081981.

Draebing, Daniel, and Till Mayer. "Topographic and Geologic Controls on Frost Cracking in Alpine Rockwalls." *Journal of Geophysical Research: Earth Surface* 126, no. 6 (2021): e2021JF006163. https://doi.org/10.1029/2021JF006163.

Fan, Xuanmei, Gianvito Scaringi, Oliver Korup, et al. “Earthquake-Induced Chains of Geologic Hazards: Patterns, Mechanisms, and Impacts.” *Reviews of Geophysics* 57, no. 2 (2019): 421–503. https://doi.org/10.1029/2018RG000626.

Fee, David, and Robin S. Matoza. “An Overview of Volcano Infrasound: From Hawaiian to Plinian, Local to Global.” *Journal of Volcanology and Geothermal Research* 249 (January 2013): 123–39. https://doi.org/10.1016/j.jvolgeores.2012.09.002.

Gardner, J. S. “Rockfall Frequency and Distribution in the Highwood Pass Area, Canadian Rocky Mountains.” *Zeitschrift Für Geomorphologie* 27, no. 3 (1983): 311–24. https://doi.org/10.1127/zfg/27/1983/311.

Glenn, Nancy F., David R. Streutker, D. John Chadwick, Glenn D. Thackray, and Stephen J. Dorsch. “Analysis of LiDAR-Derived Topographic Information for Characterizing and Differentiating Landslide Morphology and Activity.” *Geomorphology* 73, nos. 1–2 (2006): 131–48. https://doi.org/10.1016/j.geomorph.2005.07.006.

Hales, T. C., and J. J. Roering. “A Frost ‘Buzzsaw’ Mechanism for Erosion of the Eastern Southern Alps, New Zealand.” *Geomorphology* 107, nos. 3–4 (2009): 241–53. https://doi.org/10.1016/j.geomorph.2008.12.012.

Imaizumi, Fumitoshi, Norikazu Matsuoka, Yuichi S. Hayakawa, Dahal Samikshya, and Markus Stoffel. “Linkages between Abundant Rockfall and Debris-Flow Activity at Täschgufer, Swiss Alps.” *Geomorphology* 490 (December 2025): 110009. https://doi.org/10.1016/j.geomorph.2025.110009.

Johnson, J. B., J. F. Anderson, H. P. Marshall, S. Havens, and L. M. Watson. “Snow Avalanche Detection and Source Constraints Made Using a Networked Array of Infrasound Sensors.” *Journal of Geophysical Research: Earth Surface* 126, no. 3 (2021): 3. https://doi.org/10.1029/2020JF005741.

Johnson, Jeffrey B., and Timothy J. Ronan. “Infrasound from Volcanic Rockfalls.” *Journal of Geophysical Research: Solid Earth* 120, no. 12 (2015): 12. https://doi.org/10.1002/2015JB012436.

Keefer, David K. “Landslides Caused by Earthquakes.” *Geological Society of America Bulletin* 95, no. 4 (1984): 406. https://doi.org/10.1130/0016-7606(1984)95%253C406:LCBE%253E2.0.CO;2.

Kogelnig, Arnold, Johannes Hübl, Emma Suriñach, Ignasi Vilajosana, and Brian W. McArdell. “Infrasound Produced by Debris Flow: Propagation and Frequency Content Evolution.” *Natural Hazards* 70, no. 3 (2014): 3. https://doi.org/10.1007/s11069-011-9741-8.

Krautblatter, M., and M. Moser. “A Nonlinear Model Coupling Rockfall and Rainfall Intensity Based on a Four Year Measurement in a High Alpine Rock Wall (Reintal, German Alps).” *Natural Hazards and Earth System Sciences* 9, no. 4 (2009): 1425–32. https://doi.org/10.5194/nhess-9-1425-2009.

Krautblatter, Michael, and Richard Dikau. “Towards a Uniform Concept for the Comparison and Extrapolation of Rockwall Retreat and Rockfall Supply.” *Geografiska Annaler: Series A, Physical Geography* 89, no. 1 (2007): 21–40. https://doi.org/10.1111/j.1468-0459.2007.00305.x.

Krautblatter, Michael, Daniel Funk, and Friederike K. Günzel. “Why Permafrost Rocks Become Unstable: A Rock–Ice-mechanical Model in Time and Space.” *Earth Surface Processes and Landforms* 38, no. 8 (2013): 876–87. https://doi.org/10.1002/esp.3374.

Leine, R. I., A. Schweizer, M. Christen, J. Glover, P. Bartelt, and W. Gerber. "Simulation of Rockfall Trajectories with Consideration of Rock Shape." *Multibody System Dynamics* 32, no. 2 (2014): 241–71. https://doi.org/10.1007/s11044-013-9393-4.

Liu, Dunlong, Qian Wu, Hanchuan Dong, Xiaopeng Leng, Lei He, and Yan Gao. "Construction and Application of Debris Flow Infrasound Real-Time Monitoring and Warning Visualization Platform." *Natural Hazards* 112, no. 1 (2022): 1. https://doi.org/10.1007/s11069-021-05192-9.

Lyons, John, David Fee, Weston A. Thelen, Alexandra M. Iezzi, and Aaron G. Wech. *Infrasound for Volcano Monitoring*. Scientific Investigations Report. Scientific Investigations Report. 2024.

Mamot, Philipp, Samuel Weber, Tanja Schröder, and Michael Krautblatter. "A Temperature- and Stress-Controlled Failure Criterion for Ice-Filled Permafrost Rock Joints." *The Cryosphere* 12, no. 10 (2018): 3333–53. https://doi.org/10.5194/tc-12-3333-2018.

Marc, O., N. Hovius, P. Meunier, T. Uchida, and S. Hayashi. "Transient Changes of Landslide Rates after Earthquakes." *Geology* 43, no. 10 (2015): 883–86. https://doi.org/10.1130/G36961.1.

Matoza, Robin S., Michael A. H. Hedlin, and Milton A. Garcés. "An Infrasound Array Study of Mount St. Helens." *Journal of Volcanology and Geothermal Research* 160, nos. 3–4 (2007): 249–62. https://doi.org/10.1016/j.jvolgeores.2006.10.006.

Matsuoka, Norikazu. "A Multi-Method Monitoring of Timing, Magnitude and Origin of Rockfall Activity in the Japanese Alps." *Geomorphology* 336 (July 2019): 65–76. https://doi.org/10.1016/j.geomorph.2019.03.023.

Matsuoka, Norikazu. "Direct Observation of Frost Wedging in Alpine Bedrock." *Earth Surface Processes and Landforms* 26, no. 6 (2001): 601–14. https://doi.org/10.1002/esp.208.

Matsuoka, Norikazu. "Frost Weathering and Rockwall Erosion in the Southeastern Swiss Alps: Long-Term (1994–2006) Observations." *Geomorphology* 99, nos. 1–4 (2008): 353–68. https://doi.org/10.1016/j.geomorph.2007.11.013.

Matsuoka, Norikazu, and Hiroaki Sakai. "Rockfall Activity from an Alpine Cliff during Thawing Periods." *Geomorphology* 28, nos. 3–4 (1999): 309–28. https://doi.org/10.1016/S0169-555X(98)00116-0.

McColl, Samuel T. "Paraglacial Rock-Slope Stability." *Geomorphology* 153–154 (June 2012): 1–16. https://doi.org/10.1016/j.geomorph.2012.02.015.

Murton, Julian B., Rorik Peterson, and Jean-Claude Ozouf. "Bedrock Fracture by Ice Segregation in Cold Regions." *Science* 314, no. 5802 (2006): 1127–29. https://doi.org/10.1126/science.1132127.

Rempel, Alan W., Jill A. Marshall, and Joshua J. Roering. "Modeling Relative Frost Weathering Rates at Geomorphic Scales." *Earth and Planetary Science Letters* 453 (November 2016): 87–95. https://doi.org/10.1016/j.epsl.2016.08.019.

Rengers, F. K., Jason W. Kean, Nadine G. Reitman, Joel B. Smith, Jeffrey A. Coe, and Luke A. McGuire. "The Influence of Frost Weathering on Debris Flow Sediment Supply in an Alpine Basin." *Journal of Geophysical Research: Earth Surface* 125, no. 2 (2020): e2019JF005369. https://doi.org/10.1029/2019JF005369.

Sanders, Johnny W., Kurt M. Cuffey, Jeffrey R. Moore, Kelly R. MacGregor, and Jeffrey L. Kavanaugh. "Periglacial Weathering and Headwall Erosion in Cirque Glacier Bergschrunds." *Geology* 40, no. 9 (2012): 779–82. https://doi.org/10.1130/G33330.1.

Schaefer, L. N., J. A. Coe, K. Wikstrom Jones, et al. "Kinematic Evolution of a Large Paraglacial Landslide in the Barry Arm Fjord of Alaska." *Journal of Geophysical Research: Earth Surface* 128, no. 11 (2023): e2023JF007119. https://doi.org/10.1029/2023JF007119.

Wachino, Ian D., Joshua J. Roering, Reuben Cash, and Annette I. Patton. "Characterizing Geologic and Climatic Controls on Rockfall Hazards Using an Inventory and Integrated Kinematic and Runout Model: Skagway, Alaska, USA." *Natural Hazards and Earth System Sciences* 26, no. 3 (2026): 1435–56. https://doi.org/10.5194/nhess-26-1435-2026.

Watson, L. W., A. Miller, J. F. Anderson, L. Toney, and A. Ardid. "Detecting Snow Avalanche Activity Using Infrasound: Hooker Valley, New Zealand." *New Zealand Journal of Geology and Geophysics* 69, no. 1 (2026): e70015. https://doi.org/10.1002/jgo2.70015.

Watson, Leighton M., Brad Carpenter, Kevin Thompson, and Jeffrey B. Johnson. "Using Local Infrasound Arrays to Detect Plunging Snow Avalanches along the Milford Road, New Zealand (Aotearoa)." *Natural Hazards* 111, no. 1 (2022): 1. https://doi.org/10.1007/s11069-021-05086-w.

Watson, Leighton M., Alexandra M. Iezzi, Liam Toney, et al. "Volcano Infrasound: Progress and Future Directions." *Bulletin of Volcanology* 84, no. 5 (2022): 44. https://doi.org/10.1007/s00445-022-01544-w.

Whalley, W. B. *Rockfalls*. 1998.

Williams, Jack G., Nick J. Rosser, Richard J. Hardy, Matthew J. Brain, and Ashraf A. Afana. "Optimising 4-D Surface Change Detection: An Approach for Capturing Rockfall Magnitude–Frequency." *Earth Surface Dynamics* 6, no. 1 (2018): 101–19. https://doi.org/10.5194/esurf-6-101-2018.

Zimmer, Valerie L., and Nicholas Sitar. "Detection and Location of Rock Falls Using Seismic and Infrasound Sensors." *Engineering Geology* 193 (July 2015): 49–60. https://doi.org/10.1016/j.enggeo.2015.04.007.